Design of Efficient Resonator-Enhanced Electro-Optic Frequency Comb Generators

Brandon Buscaino, *Student Member, IEEE*, Mian Zhang, *Member, IEEE*, Marko Lončar, *Senior Member, IEEE, Fellow, OSA*, and Joseph M. Kahn, *Fellow, IEEE*

***Abstract*—Resonator-enhanced electro-optic (RE-EO) frequency comb generators produce broad combs by coupling an optical field to a resonator containing a phase modulator driven at a harmonic of the resonator free spectral range (FSR). Recent advances in integration technologies have opened up the possibility of fabricating low-loss, efficient, and tunable ring-based RE-EO comb generators. In this work, we analyze the properties of a canonical ring-based RE-EO comb generator and propose a new dual-ring comb generator to increase comb conversion efficiency, an especially important characteristic for comb-based optical communications systems. After a brief review of RE-EO comb generator properties in the case of resonant operation, i.e., when the optical frequency and the modulation frequency are harmonics of the resonator FSR, we analyze the effect of input optical phase noise and modulation phase noise on the resulting comb. Additionally, we show analytically that in non-resonant operation the optical frequency offset and the modulation frequency offset can be much larger than the linewidth of the resonator, increasing the tolerance to fabrication errors. Then, we develop and validate numerical models to predict the output spectrum in the presence of dispersive waveguides, which cannot be modeled analytically. Using these accurate models, we analyze a dual-ring RE-EO comb generator that uses a small coupling ring to increase the conversion efficiency to 32%, compared to the 1.3% efficiency of a single-ring RE-EO comb generator. We then analyze a point-to-point inter-data center optical link and determine that a dual-ring RE-EO comb generator can support high-capacity coherent links at 20 Tb/s per fiber.**

***Index Terms*—Electro-optic modulation, integrated optics, optical communications, optical frequency combs.**

I. Introduction

OPTICAL frequency combs have uses ranging from metrology and precision time-keeping to spectroscopy and optical communications [1]–[3]. Often, these varied applications require combs with vastly different characteristics. For example, precision timing applications require combs that span a full octave [4], while applications in spectroscopy and optical communications often require combs whose frequency spacing can be easily changed [5]. For use in optical communications, the primary application of this paper, combs may have narrower width than in other applications but must be flat and have high optical power.

Optical frequency combs can be generated by several different methods. Mode-locked lasers, for example, can output wide combs in different wavelength ranges [6]. Frequency combs can also be generated through parametric generation, via the $\chi^{(3)}$ nonlinearity in optical fibers or resonant structures [7]–[9]. Recently, comb generators based on high-Q nonlinear resonators have garnered considerable attention due to their desirable output properties [10], [11]. However, the formation dynamics of these comb generators is complex and their noise properties are still not fully understood [12], [13]. Finally, flat and high-power combs useful for optical communications can be generated by electro-optic (EO) modulation of a single-frequency optical field [14], [15], but the electrical power consumption of these comb generators is often too high [16].

Resonator-enhanced electro-optic (RE-EO) comb generators, which couple light into free-space or fiber-based resonators containing an EO modulator, have been studied for over four decades [17]–[19] and are more efficient than comb generators based on cascaded modulation [20]. Early RE-EO comb generators, implemented in lossy free-space resonators with bulky components [18], [21], [22], are sensitive to fluctuations in the input optical frequency and modulation frequency, increasing the locking requirements of the comb generator [20]. Recent advances in low-loss integrated technologies have enabled RE-EO comb generators whose modulation frequency can equal the resonator free spectral range (FSR), corresponding to a different regime of operation [23]–[25]. The effects due to a non-resonant input optical frequency and modulation frequency have been discussed in experimental contexts before [19], [26], but an exact analytical form for the output has not been determined.

Additionally, low coupling between the input optical field and the resonator is crucial to ensure that the intra-resonator optical field is modulated many times before being output-coupled, but results in conversion efficiencies less than 5% [19]. This low conversion efficiency is common amongst most resonator-based comb generators, including those made from materials

Manuscript received May 24, 2019; revised October 31, 2019 and January 5, 2020; accepted February 10, 2020. Date of publication February 13, 2020; date of current version March 17, 2020. This work was supported by Facebook, Maxim Integrated and National Science Foundation under Grant ECCS-1740291 E2CDA. *(Corresponding author: Brandon Buscaino.)*

Brandon Buscaino and Joseph M. Kahn are with the E. L. Ginzton Laboratory, Department of Electrical Engineering, Stanford University, Stanford, CA 94305 USA (e-mail: buscaino@stanford.edu; jmk@ee.stanford.edu).

Mian Zhang is with the John A. Paulson School of Engineering and Applied Sciences, Harvard University, Cambridge, MA 02138 USA, and also with HyperLight Corporation, 501 Massachusetts Ave, Cambridge, MA 02139 USA (e-mail: mianzhang@g.harvard.edu).

Marko Lončar is with the John A. Paulson School of Engineering and Applied Sciences, Harvard University, Cambridge, MA 02138 USA (e-mail: loncar@seas.harvard.edu).

Color versions of one or more of the figures in this article are available online at http://ieeexplore.ieee.org.

Digital Object Identifier 10.1109/JLT.2020.2973884

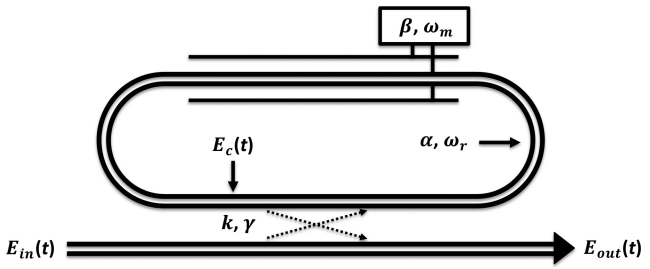

Fig. 1. Resonator-enhanced electro-optic (RE-EO) frequency comb generator. Light is coupled into the resonator with coupler power transmission k and power insertion loss γ. In the resonator with FSR ω_r the light experiences round trip power loss $(1-\alpha)$ and ideal, lumped phase modulation with modulation frequency ω_m and modulation index β. The intra-resonator field $E_c(t)$ is discussed in detail in Section IV-B.

with high $\chi^{(3)}$ nonlinearity. Nevertheless, free-space RE-EO comb generators with higher conversion efficiencies have been experimentally demonstrated by including an additional coupling resonator before the comb-generating resonator [27], [28]. While this concept is common for free-space comb generators, a dual-resonator design tailored to integrated ring-resonators is not well-known.

In this work, we derive an analytical model for the output spectrum and noise properties of a ring-based RE-EO comb generator in resonant and non-resonant operation, i.e., when the optical and modulation frequencies are resonant and non-resonant with the FSR, respectively. To model frequency-dependent propagation such as dispersion, which cannot be modeled by the first analytical model, we develop and validate two additional models, one analytical and one numerical, to determine the output comb spectrum. To increase the output optical power of the comb, we propose a dual-ring RE-EO comb generator that is composed of a small coupling ring, which traps light at the input optical frequency and a larger comb-generating ring that contains a phase modulator. This dual-ring comb generator design offers an average increase in comb line power of 14 dB compared to a single-ring comb generator and meets the optical signal-to-noise ratio (OSNR) requirements of an inter-data center wavelength-division-multiplexed (WDM) optical communications link.

The structure of this paper is as follows. Section II briefly reviews previous work on ring-based RE-EO comb generators and extends that analysis to predict the output power spectrum and noise properties of RE-EO comb generators in resonant operation. Section III analyzes the output comb properties of a non-resonant RE-EO comb generator. Section IV introduces two methods of approximating the output spectrum in the presence of frequency-dependent effects, such as dispersion. Section V proposes a design for a dual-ring RE-EO comb generator and demonstrates its utility for optical communications systems. Section VI provides a brief conclusion.

II. Resonant Operation

This section analyzes the output properties of an RE-EO comb generator when both the input optical frequency and the modulation frequency are resonant. Fig. 1 illustrates a canonical RE-EO comb generator based on a ring resonator. A single-frequency optical field $E_{\rm in}(t) = \hat{E}_{\rm in} e^{i\omega_0 t}$ is coupled into a resonator that contains a phase modulator. Once inside the low-loss resonator, light passes through the phase modulator many times, accumulating a sinusoidal time-dependent phase, before being output-coupled into the original waveguide. The complex output optical field, $E_{\rm out}(t)$, can be expressed as an infinite sum of time-shifted, phase-modulated copies of the input optical field [18]

$$E_{\rm out}(t) = \sqrt{(1-\gamma)(1-k)}E_{\rm in}(t) - k\sqrt{\frac{1-\gamma}{1-k}}\sum_{n=1}^{\infty} r^n e^{i\beta F_n(\omega_m t)} E_{\rm in}(t-nT), \quad (1)$$

where the parameters k and γ are the coupler power transmission and the power insertion loss, respectively. The resonator has a FSR of ω_r at the input optical frequency ω_0 and round-trip time $T = 2\pi/\omega_r$. The cumulative round-trip field gain is $r = \sqrt{\alpha(1-\gamma)(1-k)}$, where the light experiences round-trip power loss $(1-\alpha)$. Ideal, lumped phase modulation occurs at modulation frequency ω_m and modulation index β. We define a cascaded modulation function

$$F_n(\omega_m t) = \sum_{i=1}^{n} \sin \omega_m (t - iT), \quad (2)$$

where the term $\beta F_n(\omega_m t)$ is the accumulated time-dependent phase of the internal field in its nth round trip. Notably, the second term in (1) contains an additional factor of $\sqrt{k/(1-k)}$ compared to the derivation in [18].

When the optical input frequency and the modulation frequency are resonant with the FSR ($\omega_0 T$ and $\omega_m T$ are integer multiples of 2π, respectively), the output optical field is [18]

$$E_{\rm out}(t) = \sqrt{(1-\gamma)(1-k)}\hat{E}_{\rm in} e^{i\omega_0 t} - k\sqrt{\frac{1-\gamma}{1-k}}\frac{r e^{i\beta \sin \omega_m t}}{1 - r e^{i\beta \sin \omega_m t}} \hat{E}_{\rm in} e^{i\omega_0 t}. \quad (3)$$

Fig. 2(a) shows the intra-resonator power spectrum for $k = 0.03$, $\gamma = 0$, $\alpha = 0.95$, $\beta = \pi/2$, and $P_{\rm in} = |\hat{E}_{\rm in}|^2 = 1$. These values are consistent with state-of-the-art fabrication technology [23], [29] and unless otherwise noted, these are the default parameters used for the rest of this paper. The intra-resonator optical field is composed of hundreds of single-frequency components spaced at the modulation frequency, with a large dip at the center frequency. The output comb, however, has a large peak at the input optical frequency due to the unmodulated light that passes through the coupler. The horizontal axis in Fig. 2(a) is frequency, normalized to the resonator FSR (i.e., $p = \omega/\omega_r$). In following figures, when comb spectra are plotted, we omit the vertical lines that indicate the comb is composed of distinct frequency components and instead show only the comb envelope.

Fig. 2(b) shows the intra-resonator temporal power profile. Inside the resonator, phase modulation induces pulse formation when the previously mentioned resonant conditions are satisfied. Notably, while the periodicity of the temporal power profile is twice the modulation frequency, the periodicity of the

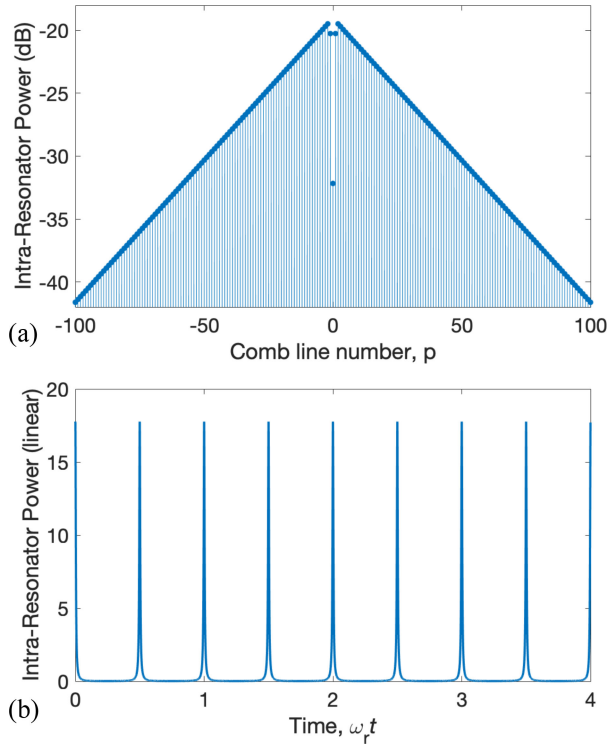

Fig. 2. Properties of the intra-resonator field of a RE-EO comb generator. (a) Power spectrum of the intra-resonator optical field. (b) Temporal power profile inside the resonator, demonstrating pulse formation.

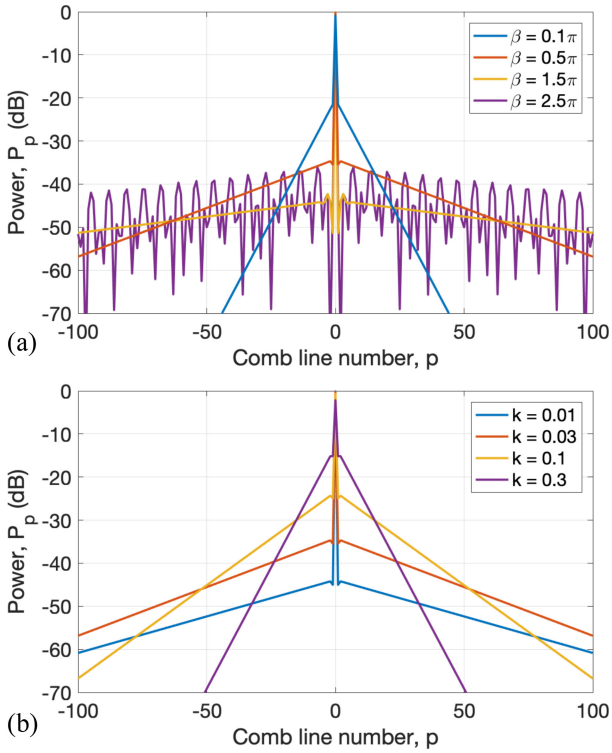

Fig. 3. Comb spectra as a function of comb line number p for various parameters. (a) Comb spectra P_p for different modulation indices β. For $\beta > 2\pi$, the output comb is highly non-uniform and chaotic. (b) Comb spectra P_p for different coupler power transmissions k. Decreasing k increases the flatness of the comb but reduces the total comb conversion efficiency η.

optical field is equal to the modulation frequency due to the time-dependent phase of the output optical field [30].

A. Output Power Spectrum

Simplified analytical models have been previously developed for RE-EO comb generators based on free-space Fabry-Pérot resonators but can be adapted to RE-EO comb generators based on ring resonators. For example, the power in the pth comb line of a ring-based RE-EO comb generator is approximately ($\beta < \pi, p \neq 0$) [19]

$$P_p \propto e^{\frac{-|p|(1-r^2)}{\beta}}. \tag{4}$$

Increasing the modulation index β and round-trip field gain r results in broader comb formation.

An analytical solution valid for all cases can be determined when both the input optical frequency and modulation frequency are resonant. By applying a Jacobi-Anger expansion [31] to (1), the output optical field is

$$E_{\text{out}}(t) = \sqrt{(1-\gamma)(1-k)}\hat{E}_{\text{in}}e^{i\omega_0 t} - k\sqrt{\frac{1-\gamma}{1-k}}\hat{E}_{\text{in}}\sum_{p=-\infty}^{\infty}\sum_{n=1}^{\infty} r^n J_p(\beta n)e^{i(\omega_0+p\omega_m)t}, \tag{5}$$

where J_p is the pth order Bessel function of the first kind. The power in the pth comb line is then

$$P_p = (1-\gamma)(1-k)P_{\text{in}}\left|\delta_p - \frac{k}{1-k}\sum_{n=1}^{\infty} r^n J_p(\beta n)\right|^2, \tag{6}$$

where δ_p is the Kronecker delta.

Fig. 3(a) shows output spectra of a RE-EO comb generator for various modulation indices. As expected, increasing the modulation index decreases the overall slope of the comb spectrum. However, for large modulation indices ($\beta > 2\pi$), the profile of the spectrum becomes nonuniform due to the highly oscillatory nature of the Bessel function in (6). Analytical models exist for free-space RE-EO comb generators driven with large modulation indices [20], but they will not be discussed further here because applications in optical communications often require a uniform and flat comb spectra.

Fig. 3(b) shows output spectra of a RE-EO comb generator for different coupling power transmissions k with the same parameters as Fig. 3(a). Since the intra-resonator power loss $(1-\alpha)$ and the coupler insertion loss γ are often fixed, the coupler power transmission k can be tuned to change the output spectrum. As k is decreased, the comb slope decreases because the intra-resonator field is modulated during more round trips before being output-coupled. However, decreasing k also decreases the efficiency $\eta = \sum_{p\neq 0} P_p/P_{\text{in}}$ of the comb generation

process because more of the input optical field is passed through the coupler and into the output waveguide.

Notably, the spectra shown in Fig. 3 contain large peaks at the input frequency because a majority of the light is transmitted through the waveguide. This peak could be eliminated by including an additional waveguide coupled to the resonator. However, an additional waveguide would increase the round-trip loss $(1 - r^2)$, decreasing the slope of the comb according to (4). While the large peak in the spectrum is not ideal for applications that require a flat comb, such as optical communications, optical filters to flatten the spectrum can be employed, as will be discussed in Section V-C. Moreover, in Section V we propose a RE-EO comb generator design that utilizes a ring coupler to increase the power-conversion efficiency and remove the peak from the output spectrum.

B. Output Noise

1) Optical Input Phase Noise: Previously, we assumed that the input optical field contained a single frequency. We now relax this assumption and assume that the input field is $E_{\text{in}}(t) = \hat{E}_{\text{in}} e^{i\omega_0 t + i\theta_o(t)}$ where $\theta_o(t)$ is the phase noise of the input optical field. The power spectral density (PSD) of $E_{\text{in}}(t)$ is [32]

$$S_{\text{in}}(\omega) = \int_{-\infty}^{\infty} \langle E_{\text{in}}(t) E_{\text{in}}^*(t+\tau)\rangle e^{-i\omega\tau} d\tau$$
$$= P_{\text{in}} \int_{-\infty}^{\infty} \langle e^{i\Delta_\tau \theta_o}\rangle e^{-i(\omega+\omega_0)\tau} d\tau, \tag{7}$$

where $\langle\cdot\rangle$ denotes averaging over time t, and $\Delta_\tau\theta_o = \theta_o(t+\tau) - \theta_o(t)$ [33].

When both the input optical frequency and the modulation frequency are resonant, the output PSD of the pth comb line in the presence of input optical phase noise is

$$S_{out,p}(\omega) = k^2 \frac{1-\gamma}{1-k} \left|\chi_p(\omega)\right|^2 S_{\text{in}}(\omega - p\omega_m), \tag{8}$$

where the frequency-dependent linewidth correction term for the pth comb line is

$$\chi_p(\omega) = \sum_{n=1}^{\infty} r^n J_p(\beta n) e^{-i\omega n T}. \tag{9}$$

From (8), it is evident that multiplication by $|\chi_p(\omega)|^2$ changes the shape of the PSD of the pth comb line phase noise. The calculations to derive this result are included in Appendix A and are complementary to previous work [34].

Fig. 4 plots the normalized linewidth correction factor $|\chi_p(\omega)|^2$ for various comb lines. The horizontal axis is frequency from the center of the pth comb line, normalized to the resonator FSR. For many practical ring resonators, the FSR can be over four orders of magnitude larger than the linewidth of the input optical carrier. For this reason, only the shape of $|\chi_p(\omega)|^2$ near $\omega = \omega_0 + p\omega_m$ contributes to a change in linewidth. From the vertical scale of Fig. 4 it is clear that the linewidth correction term is locally flat for frequencies within the linewidth of the input optical field. For this reason, the phase noise of the pth comb line is nearly identical to the phase noise of the input optical field.

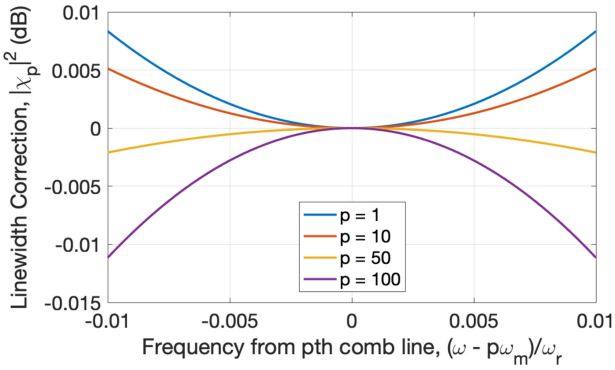

Fig. 4. Linewidth correction factor $|\chi_p(\omega)|^2$ for various comb line numbers p. Because $|\chi_p(\omega)|^2$ is locally flat for ω inside the input optical linewidth, the input optical phase noise is approximately copied to each of the comb lines.

2) Modulation Phase Noise: Similar to the previous section, the impact of modulator phase noise can be analyzed by introducing a time-dependent phase $\theta_e(t)$ into the phase modulation. The cascaded modulation function, including modulation phase noise is

$$F_n(\omega_m t) = \sum_{i=1}^{n} \sin\left[\omega_m(t - iT) + \theta_e(t - iT)\right]$$
$$\approx n \sin\left[\omega_m t + \theta_e(t)\right], \tag{10}$$

where we have assumed that $\theta_e(t)$ is slowly varying over relevant resonator time scales such as the resonator decay lifetime. This is a safe assumption because crystal-controlled microwave oscillators used for modulation have coherence times much longer than those of optical resonators [35].

By inserting (10) into (1) and assuming resonance of the input optical frequency and modulation frequency, the output field of the pth comb line ($p \neq 0$) is

$$E_p(t) = -k\sqrt{\frac{1-\gamma}{1-k}}\hat{E}_{\text{in}} \left[\sum_{n=1}^{\infty} r^n J_p(\beta n)\right]$$
$$\times e^{i(\omega_0 + p\omega_m)t + ip\theta_e(t)}. \tag{11}$$

The PSD of the pth comb line in the presence of modulation phase noise is then

$$S_{out,p}(\omega) = P_p \int_{-\infty}^{\infty} \langle e^{ip\Delta_\tau\theta_e}\rangle e^{-i\omega\tau} d\tau, \tag{12}$$

where P_p is given by (6) and $\Delta_\tau\theta_e = \theta_e(t+\tau) - \theta_e(t)$. If we assume that $\Delta_\tau\theta_e$ is a Gaussian random process, then the linewidth of the pth optical field, $\Delta\omega_p$, is related to the phase noise by [33]

$$\Delta\omega_p|\tau| = \langle (p\Delta_\tau\theta_e)^2\rangle. \tag{13}$$

From this relation, it is clear that the linewidth of the pth comb line increases quadratically with p.

The quadratic dependence of the linewidth on comb line number can introduce significant noise for applications that require thousands of comb lines, such as precision timing. However, for applications that require hundreds of comb lines or less, the

output phase noise is still dominated by input laser phase noise. Recent experimental work has shown that high-frequency comb line phase noise can be filtered by inputting an optical frequency slightly detuned away from a harmonic of the FSR [36]. This effect results from a frequency-dependent filtering term in (11), though a detailed analysis is not presented here.

III. Non-Resonant Operation

In the previous section we assumed that both the input optical frequency and the modulation frequency were harmonics of the resonator FSR. In practical systems, this assumption is not always satisfied. In order to maintain this resonance condition, various locking methods have been proposed to ensure that the desired comb properties are preserved [18], [19]. Here, since the most important comb property for optical communications is comb power, we analyze impairments to the output spectrum in the presence of optical frequency offsets and modulation frequency offsets. Importantly, the absolute and relative phases of the comb lines will change as well [37], but we will not discuss that effect further here.

A. Non-Resonant Optical Input

We first assume that the input field has an optical frequency offset $\Delta\omega_o$ such that the input optical field is $E_{\text{in}}(t) = \hat{E}_{\text{in}} e^{i(\omega_0+\Delta\omega_o)t}$. We define the normalized optical frequency offset $\phi_o = \Delta\omega_o T$. From (1), the output power in the pth comb line in the presence of an input optical frequency offset is

$$P_{p,o} = k^2 \frac{1-\gamma}{1-k} P_{\text{in}} \left| \sum_{n=1}^{\infty} (re^{-i\phi_o})^n J_p(\beta n) \right|^2. \tag{14}$$

Fig. 5(a) shows the output comb spectrum calculated from (14) for various values of ϕ_o. For small values of ϕ_o, the shape of the comb remains unchanged, while for values of ϕ_o that approach and surpass the modulation index β, the comb drastically decreases in size.

For unmodulated resonators, inputting an optical frequency within the resonator linewidth $\Delta\omega_r = (1-r^2)\omega_r/(2\pi)$ is critical to increasing the built-up power in the resonator. Thus, one might expect that inputting an optical frequency outside of $\Delta\omega_r$ into a modulated resonator may reduce the comb generation efficiency. Indeed for some values of ϕ_o, such as $\phi_o > 0.5\pi$, the output comb is much less flat. However, flat combs can be generated even in the presence of normalized optical frequency offsets greater than the normalized resonator linewidth, $\phi_r = \Delta\omega_r T = (1-r^2)$. For the default parameters assumed in this paper, $\phi_r = 0.013\pi$, while broad comb formation is evident for $\phi_o = 0.25\pi$ in Fig. 5(a). These results agree with previous experimental results from free-space RE-EO comb generators [30]. An explanation for this phenomenon is discussed in Section IV-A.

B. Non-Resonant Modulation

We now assume that the modulator is driven with modulation frequency offset $\Delta\omega_m$ and define the normalized modulation frequency offset $\phi_m = \Delta\omega_m T$. From (1), the power in the pth comb line in the presence of a modulation frequency offset is

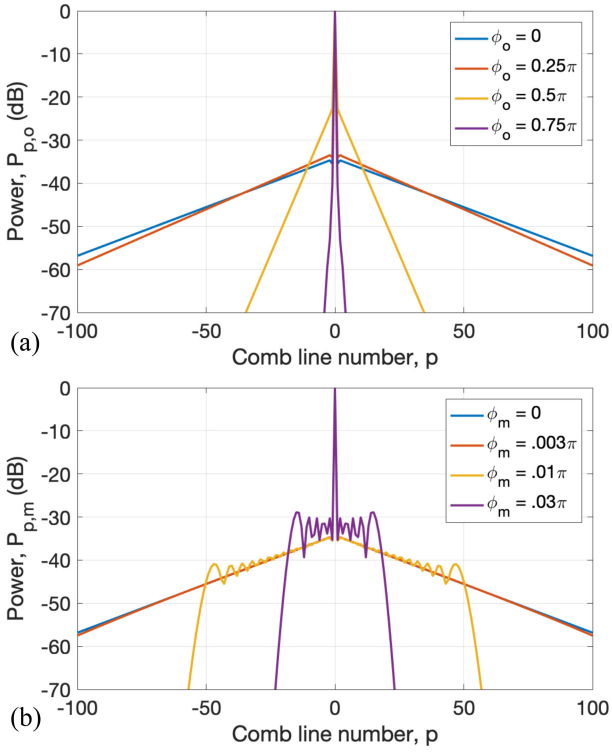

Fig. 5. Output spectra from a non-resonant RE-EO comb generator. (a) Power spectra $P_{p,o}$ for different optical frequency offsets. For $\phi_o > \beta$, the comb width is reduced substantially. (b) Power spectra $P_{p,m}$ for different modulation frequency offsets, demonstrating reduction of comb width for large ϕ_m.

$$P_{p,m} = \frac{(1-\gamma)}{(1-k)} k^2 P_{\text{in}} \times \left| \sum_{n=1}^{\infty} \sum_{q=-\infty}^{\infty} r^n i^q J_{p-q}(\beta_o(\phi_m, n)) J_q(\beta_e(\phi_m, n)) \right|^2, \tag{15}$$

where we have defined the modified odd and even modulation indices $\beta_o(\phi_m, n)$ and $\beta_e(\phi_m, n)$ as

$$\beta_o(\phi_m, n) = \beta\left(\frac{1}{2}\cot(\phi_m/2) - \frac{\cos\left((n+\frac{1}{2})\phi_m\right)}{2\sin(\phi_m/2)} \right) \tag{16}$$

$$\beta_e(\phi_m, n) = \beta\left(-\frac{1}{2} + \frac{\sin\left((n+\frac{1}{2})\phi_m\right)}{2\sin(\phi_m/2)} \right). \tag{17}$$

The calculations to derive (15) from (1) are included in Appendix B. Since (15) introduces an additional infinite summation, the complexity of the calculation increases significantly, especially in cases where the resonator loss is small or modulation index is large. In Section IV-B we develop an efficient numerical model that approximates this analytical model.

Fig. 5(b) shows comb spectra in the presence of various modulation frequency offsets. For small modulation frequency offsets, the comb remains flat. However, an increase in ϕ_m from $\phi_m = 0.01\pi$ to $\phi_m = 0.03\pi$, leads to a proportional decrease of the total width from approximately 120 comb lines to 40 comb

lines. Similar to Section III-A, the comb spectra in Fig. 5 exhibit behavior that deviates from the behavior of an unmodulated resonator. Comb lines with frequencies that lie far outside of the resonator linewidth still build up in the resonator. For example, for $\phi_m = 0.03\pi$, all of the approximately 40 generated comb frequencies lie outside of the normalized resonator linewidth, $\phi_r = 0.013\pi$.

The steep cut-off frequencies in the spectra of Fig. 5(b) are notably similar to the total spectral width of the FM laser [38]–[40]. In particular, for small modulation indices, low loss, and gainless media the total comb width is approximately $2\beta\omega_m/\phi_m$ [38]. Even for larger modulation indices, such as $\beta = 0.5\pi$ assumed here, this approximation is accurate so long as the modulation frequency offset is small compared to the resonator FSR ($\Delta\omega_m T \ll 1$). For example, the calculated width of the comb spectrum for $\phi_m = 0.01\pi$ in Fig. 5(b) is $100\omega_m$. This overlaps precisely with the cutoff frequencies that occur approximately ± 50 comb lines from center.

Finally, we note two important consequences of the above: (1) large ring resonators, corresponding to large T, are much more sensitive to optical frequency offsets and modulation frequency offsets because the normalized frequency offsets are linearly dependent on the resonator length. For this reason, it is ideal for the modulation frequency to equal the fundamental FSR rather than a harmonic of the FSR in order to increase the tolerable frequency offsets; (2) the flexibility and tolerance to fabrication errors of RE-EO comb generators is much higher than other integrated comb generators. For example, a dense WDM optical communications system may require 100 comb lines spaced at 50 GHz. While the frequency spacing of integrated Kerr comb generators is limited by the fabricable FSR of the resonator, the RE-EO comb generator frequency spacing can be tuned by up to $\phi_m = \pm 0.01\pi$ to alleviate fabrication requirements, as shown by the yellow curve in Fig. 5(b). For the example above, the frequency spacing of the output comb can be tuned by 1 GHz with minimal impact on the desired comb lines.

IV. Dispersive Resonator

While the analytical model in Section III exactly predicts the output comb spectra of a RE-EO comb generator in resonant and non-resonant operation, these models cannot include arbitrary frequency-dependent effects such as dispersion. In this section, we develop two methods, one analytical and one numerical, for approximating the output spectrum of a dispersive RE-EO comb generator. We then compare all three methods, which are in excellent agreement.

A. Round-Trip Phase Model

An intuitive understanding of the resonance conditions of an RE-EO comb generator can be approached first from the resonance conditions of an unmodulated resonator, resulting from interference of internal and external fields. For example, a typical resonance condition for an input optical field with frequency ω_p coupled to a resonator with normalized linewidth ϕ_r, as defined in Section III-A, is [41]

$$|\theta_{p,tot}| < \phi_r/2, \tag{18}$$

where $\theta_{p,tot} = \omega_p T \bmod 2\pi$ is the total round-trip accumulated phase offset of the optical field. Frequencies that do not satisfy this condition do not experience constructive interference inside the resonator.

However, the intra-resonator phase modulation introduces a time-dependent variation in the resonance condition that results in constructive interference at one or more locations inside the resonator, depending on whether the phase modulation is equal to, or a subharmonic of, the FSR. As a result of this spatially varying constructive interference, intra-resonator pulses are formed. The new condition for constructive interference in the resonator is then $|\theta_{p,tot} + \beta \sin\omega_m t| < \phi_r/2$. Since this condition may be satisfied for any time t the final resonance condition is

$$-\beta < \theta_{p,tot} < \beta, \tag{19}$$

where we have omitted the finite resonator linewidth because it is often much smaller than the modulation index. This resonance condition explains the comb formation effects in Section III, where comb lines were generated even though they were outside of the resonator linewidth.

To validate this model, consider a RE-EO comb generator that is modulated exactly at the resonator FSR ($\phi_m = 0$) but has some known optical frequency offset ϕ_o. In the absence of dispersion, the round-trip accumulated phase of the pth comb line is $\theta_{p,tot} = \phi_o$. For unmodulated resonators, constructive interference inside the resonator can be verified by changing the optical frequency offset and measuring a dip in the transmission spectrum. This effect can also be observed in modulated resonators where, analogous to (3), the time-dependent output field in the presence of an optical frequency offset is

$$E_{\text{out}}(t) = \sqrt{(1-\gamma)(1-k)}\hat{E}_{\text{in}}e^{i\omega_0 t} - k\sqrt{\frac{1-\gamma}{1-k}}\frac{(re^{-i\phi_o})e^{i\beta\sin\omega_m t}}{1-(re^{-i\phi_o})e^{i\beta\sin\omega_m t}}\hat{E}_{\text{in}}e^{i\omega_0 t}. \tag{20}$$

Fig. 6 shows the time-averaged output power $\langle|E_{\text{out}}(t)|^2\rangle$ as a function of the normalized optical frequency offset for various modulation indices. As expected, we observe a narrow dip in the power transmission for $\beta = 0$, corresponding to the expected output from a unmodulated resonator. For $\beta \neq 0$, however, constructive interference occurs at many values of the optical frequency offset. The dashed lines in Fig. 6 correspond to the limits of the round-trip phase model developed in this section ($-\beta < \phi_o < \beta$), which accurately predict the maximum optical frequency offset that results in intra-resonator power build-up.

The round-trip phase model can be extended to include effects such as modulation frequency offsets as well as dispersion. First, we note that in a single round trip, the accumulated phase of the pth comb line due to a modulation frequency offset, $\theta_{p,m}$, is linear in comb line number, i.e.,

$$\theta_{p,m} = \Big[\omega_0\, T + p(\omega_m + \Delta\omega_m)T\Big] \bmod 2\pi = p\phi_m. \tag{21}$$

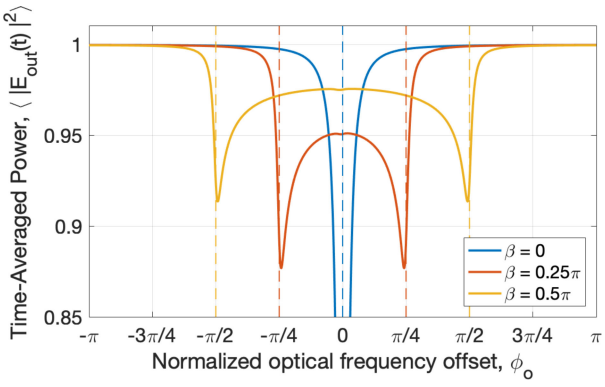

Fig. 6. Time-averaged power transmission $\langle |E_{\text{out}}(t)|^2 \rangle$ for various optical frequency offsets ϕ_o and modulation indices β. Dashed lines correspond to the edge of the round-trip phase model resonance condition as described in Section IV-A.

The effects of dispersion can also be included by integrating the measured or simulated group velocity dispersion to determine the round-trip accumulated phase offset of the pth comb line due to dispersion, $\theta_{p,d}$. However, if we assume a linear dispersion profile, $\theta_{p,d}$ is

$$\theta_{p,d} = \left[(\omega_0 + p\omega_m)T + p^2\omega_m^2 \beta_2 L \right] \bmod 2\pi = p^2\phi_d, \quad (22)$$

where $\beta_2 L$ is the round-trip group velocity dispersion and the normalized phase offset due to dispersion is then $\phi_d = \omega_m^2 \beta_2 L$.

Finally, the resonance condition for an RE-EO comb generator including optical frequency offsets, modulation frequency offsets, and linear dispersion is

$$-\beta < \phi_o + p\phi_m + p^2\phi_d < \beta. \quad (23)$$

Previous authors have derived similar expressions and analyzed the dispersion-limited comb width of free-space RE-EO comb generators using Fabry-Pérot resonators [42]. For a linear dispersion profile, the maximum comb width occurs when $\phi_o = -\beta$ and is given by $\Delta\omega_{\text{comb}} = \sqrt{\frac{2\beta}{\beta_2 L}}$. This value agrees with previous comb widths up to a factor of $\sqrt{2}$ due to the difference in FSR of a Fabry-Pérot resonator and ring resonator of identical length [26].

To fully characterize the output power spectrum, we make the following assumptions: (a) the light in the center frequency is dominated by the input field that passes through the coupler, i.e., $P_0 = (1-\gamma)(1-k)P_{\text{in}}$, (b) the slope of the comb spectrum is given by (4), and (c) the power in the first sideband is given by $P_{\pm 1} = k^2 \frac{1-\gamma}{1-k} J_1(\beta)^2$, simplified from (6). These assumptions, along with (23) form the round-trip phase model, which can efficiently predict the approximate shape of the output comb spectrum. Finally, we note that the round-trip phase model as well as the modeling in Section III have been successfully used to predict the output comb spectrum of fabricated ring-based devices [24].

B. Steady-State Matrix Method

One drawback of the round-trip phase model is that it is impossible to determine fine features in the output comb spectrum, such as in Fig. 5(b) where neighboring comb line powers can vary by over 10 dB. In this subsection, we develop a numerical method that is capable of resolving these fine features by determining a relation between the comb lines inside the resonator. Similar calculations have been performed before in the context of free-space Fabry-Pérot resonators [42], but not ring-based cavities.

First, we propagate the intra-resonator field $E_c(t)$, shown in Fig. 1, by one round-trip time T resulting in the following relation:

$$E_c(t) = \sqrt{\alpha} e^{i\beta \sin \omega_m t} \Big[\sqrt{(1-\gamma)(1-k)} E_c(t+T) + i\sqrt{(1-\gamma)k} E_{\text{in}}(t+T) \Big]. \quad (24)$$

We then assume that $E_c(t)$ can be expressed as a superposition of optical fields with frequencies spaced at the modulation frequency, i.e.,

$$E_c(t) = \sum_{p=-\infty}^{\infty} E_p e^{i(\omega_0 + p\omega_m)t}, \quad (25)$$

where E_p is the complex optical field of the pth comb line inside the resonator. If the optical field has reached steady state, corresponding to many round trips after the light is first input-coupled into the resonator, the relation between all E_p is

$$E_p = r \sum_{q=-\infty}^{\infty} J_q(\beta) E_{p-q} e^{i\theta_{p-q,tot}} + i\sqrt{\frac{k}{1-k}} r \hat{E}_{\text{in}} J_p(\beta) e^{i\theta_{0,tot}}, \quad (26)$$

where $\theta_{p,tot} = \phi_o + \theta_{p,m} + \theta_{p,d}$ is the round-trip normalized frequency offset of the pth comb line.

This system of linear equations can be solved with simple matrix methods. The output field in the waveguide is

$$E_{\text{out}}(t) = \sqrt{(1-\gamma)(1-k)} E_{\text{in}}(t) + i\sqrt{(1-\gamma)k} E_c(t), \quad (27)$$

where we have already solved for the values of the complex optical field E_p above.

In practice, when using a matrix solver to compute E_p, it is necessary to increase the number of simulated comb lines because the model may become inaccurate at the edges of the spectrum. This effect occurs because frequency conversion from carriers outside of the width of the simulation are not included. Since this method is quite efficient, increasing the number of simulated comb lines by even a factor of two is often tolerable. Although not discussed further in this paper, these equations reveal individual phase information of the comb lines, which have analytical solutions [30], [43], and may be useful for applications where relative phase information is desired.

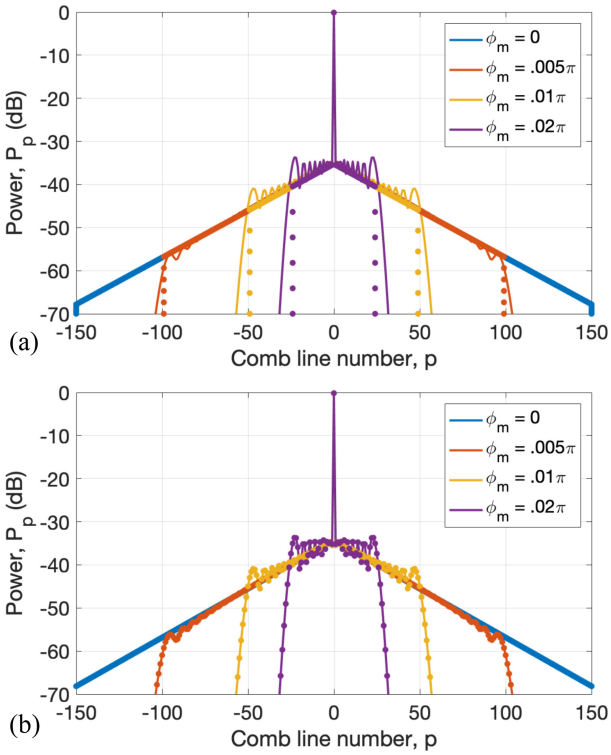

Fig. 7. Comparison of methods used to predict the output comb spectrum. (a) Output comb spectra P_p calculated with the analytical model (lines) and the round-trip phase model (filled circles) for various modulation frequency offsets. (b) Output comb spectra P_p calculated with the analytical model (lines) and the steady-state matrix method (filled circles) for various modulation frequency offsets.

C. Comparison of Methods

Here, we validate the three models of computing the output spectrum, the analytical model of Section III, the round-trip phase model of Section IV-A, and the steady-state matrix method of Section IV-B, by comparing the predicted output spectra in the presence of modulation frequency offsets. Since optical frequency offsets solely change the slope of the comb, we have omitted this comparison.

Fig. 7(a) shows the spectra calculated from the analytical model (lines) and the round-trip phase model (filled circles) for various modulation frequency offsets. The round-trip phase model accurately predicts the comb width and shape, but fails to predict the fine features of the comb spectrum, as expected. Fig. 7(b) compares the spectra computed with the analytical model (lines) and the steady-state matrix method (filled circles). Here, the steady-state matrix method is able to calculate the fine features of the comb spectrum with high accuracy.

The round-trip phase model and the steady-state matrix method can also be used to predict the effects of dispersion. In the following, we assume a linear dispersion profile (i.e., $\theta_{p,d} = p^2\phi_d$) with $\phi_d = 2\pi \times 10^{-4}$. This value of ϕ_d is considerably larger than any practical values in order to emphasize the effects of dispersion. For example, for a lithium niobate resonator with 10 GHz FSR, this value of ϕ_d would correspond to a group velocity dispersion of $\sim 1.2 \times 10^4$ fs^2/mm, over two orders of magnitude larger than that of current waveguide technology [44].

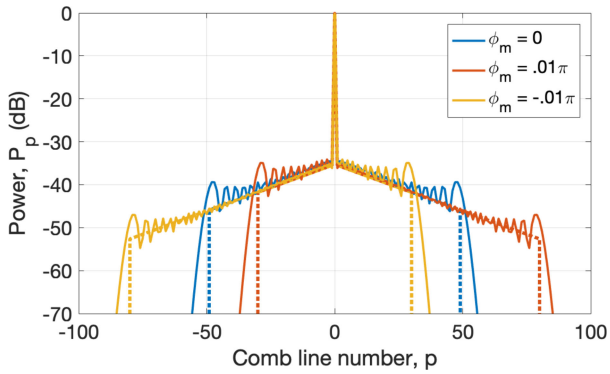

Fig. 8. Output comb spectra P_p from the round-trip phase model (dotted line) and the steady-state matrix method (solid line). In the presence of modulation frequency offsets and dispersion, complex and asymmetric comb spectra can be observed.

Fig. 8 compares output comb spectra for various modulation frequency offsets for a linear dispersion profile. As in Fig. 7, the round-trip phase model is able to predict the comb shape, but is not able to determine fine comb features. Conversely, the steady-state matrix method is able to resolve fine features in the comb spectra.

Interestingly, when both modulation frequency offsets and dispersion are included, the comb spectra becomes asymmetric about the center frequency. This effect results from the resonance condition $-\beta < p\phi_m + p^2\phi_d < \beta$, where the resonance condition for positive and negative p is different. For higher-frequency comb lines ($p > 0$), both the modulation frequency offset and the dispersion phase offset have the same sign while for lower-frequency comb lines ($p < 0$), they have opposite signs. Unlike many other comb generators, such as those based on $\chi^{(3)}$ nonlinear effects, the RE-EO comb generator does not require extensive dispersion engineering to produce viable frequency combs because it does not require phase matching over long periods of time.

V. Frequency-Dependent Coupling

As mentioned in Section II-A, resonator-based comb generators often have low efficiency due to low coupling between the input waveguide and resonator. A frequency-dependent coupler with high transmission at the input frequency, but low transmission at all other frequencies can solve this problem because the input light can efficiently couple into the resonator where the newly generated frequencies may then resonate for many round trips. While complicated frequency-dependent couplers based on photonic crystals or distributed Bragg reflectors can be fabricated to approach the desired frequency response, these methods introduce additional fabrication requirements and excess insertion loss. This section analyzes the impact on the output spectrum of an additional ring coupler used to efficiently couple the input field to the comb-generating resonator.

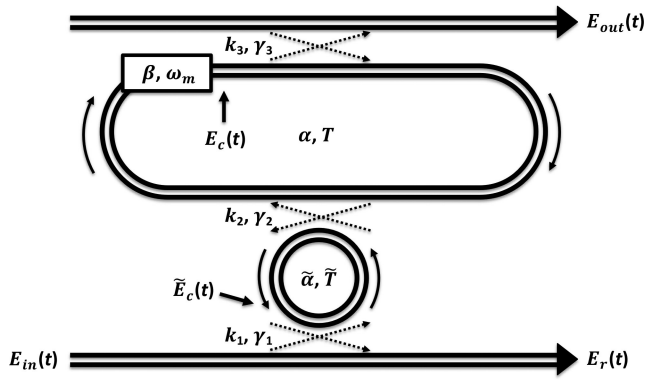

Fig. 9. Diagram of a dual-ring EO comb generator. Power at the input optical frequency builds up in the small ring and is then coupled to a larger resonator, where the comb is generated. A third coupler is used to output-couple the desired comb.

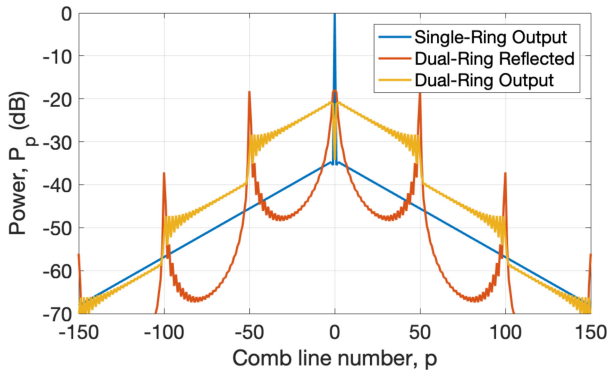

Fig. 10. Output spectra P_p of a single-ring comb generator and a dual-ring comb generator. The reflected field from the dual-ring EO comb generator is also shown, demonstrating constructive build-up at the FSR of the coupling ring.

A. Dual-Ring EO Comb Generator

Fig. 9 illustrates the proposed dual-ring EO comb generator. An input optical field $E_{\rm in}(t)$ is first resonantly coupled into a small ring. Inside that ring, power builds up at the input optical frequency, before it is coupled into the larger, comb-generating resonator. This resonator includes a coupler to output the desired frequency comb. The coupler power transmission coefficients are k_1, k_2, and k_3 and the coupler insertion losses are γ_1, γ_2, and γ_3, as shown in Fig. 9. The power losses of the small ring, $(1-\widetilde{\alpha})$, and of the comb-generating resonator, $(1-\alpha)$, are related by $\widetilde{\alpha}=\alpha^{\widetilde{T}/T}$, where $1/\widetilde{T}$ and $1/T$ are the FSRs of the small ring and comb-generating resonator, respectively.

The new output field $E_{\rm out}(t)$ can be calculated as a function of the input field $E_{\rm in}(t)$ with the steady-state matrix method. However, the small ring coupler introduces frequency-dependent phase shifts, loss, and power transmission. To determine a self-consistent relation between the comb line optical fields E_p, analogous to (26), that includes these effects, we can apply the same techniques as Section IV-B.

First, the field in the small resonator, $\widetilde{E}_c(t)$, and the field in the larger resonator, $E_c(t)$, can be related by the following equations:

$$\begin{aligned}\widetilde{E}_c(t) &= \widetilde{r}'\widetilde{E}_c(t+\widetilde{T}) \\ &\quad + i\sqrt{\frac{k_2}{1-k_2}}\left(\frac{\widetilde{\alpha}}{\alpha}\right)^{\frac{1}{4}} r' E_c(t+\widetilde{T}/2+T/2) \\ &\quad + i\sqrt{\frac{k_1}{1-k_1}}\widetilde{r}' E_{\rm in}(t+\widetilde{T}) \qquad (28)\\ E_c(t) &= r' e^{i\beta\sin\omega_m t} E_c(t+T) \\ &\quad + i\sqrt{\frac{k_2}{1-k_2}}\left(\frac{\alpha}{\widetilde{\alpha}}\right)^{\frac{1}{4}} \widetilde{r}' e^{i\beta\sin\omega_m t}\widetilde{E}_c(t+\widetilde{T}/2+T/2) \\ &\quad - (\alpha\widetilde{\alpha})^{\frac{1}{4}}\sqrt{(1-\gamma_1)k_1(1-\gamma_2)k_2}\, e^{i\beta\sin\omega_m t} \\ &\quad \times E_{\rm in}(t+\widetilde{T}/2+T/2), \qquad (29)\end{aligned}$$

where $\widetilde{r}'=\sqrt{\widetilde{\alpha}(1-\gamma_1)(1-k_1)(1-\gamma_2)(1-k_2)}$ is the round-trip gain coefficient of the small ring and $r'=\sqrt{\alpha(1-\gamma_2)(1-k_2)(1-\gamma_3)(1-k_3)}$ is the round-trip gain coefficient of the comb-generating resonator.

If we assume that both $E_c(t)$ and $\widetilde{E}_c(t)$ are superpositions of fields spaced at the modulation frequency, analogous to (25), the complex field of the pth comb line, E_p, is related to the other comb fields and input field via the following expression:

$$\begin{aligned}E_p &= \sum_{q=-\infty}^{\infty} r' J_q(\beta) e^{i\omega_{p-q}T}\left(\frac{1-\widetilde{r}' e^{i\omega_{p-q}\widetilde{T}}/(1-k_2)}{1-\widetilde{r}' e^{i\omega_{p-q}\widetilde{T}}}\right) E_{p-q} \\ &\quad - (\alpha\widetilde{\alpha})^{1/4}\sqrt{(1-\gamma_1)k_1(1-\gamma_2)k_2} \\ &\quad \times J_p(\beta) e^{i\omega_0(T/2+\widetilde{T}/2)}\left(\frac{1}{1-\widetilde{r}' e^{i\omega_0\widetilde{T}}}\right)\hat{E}_{\rm in}, \qquad (30)\end{aligned}$$

where $\omega_p T=\theta_{p,tot}$ is the accumulated round-trip phase of the pth comb line in the comb-generating resonator and $\omega_p\widetilde{T}=(\widetilde{T}/T)\theta_{p,tot}+p\omega_m\widetilde{T}$ is the round-trip accumulated phase of the pth comb line in the small ring.

The output optical field $E_{\rm out}(t)$ and the reflected field $E_r(t)$ are

$$E_{\rm out}(t)=i\sqrt{(1-\gamma_3)k_3}E_c(t) \qquad (31)$$

and

$$E_r(t)=i\sqrt{(1-\gamma_1)k_1}\widetilde{E}_c(t)+\sqrt{(1-\gamma_1)(1-k_1)}E_{\rm in}(t). \qquad (32)$$

With these expressions, we can utilize a simple matrix solver to first calculate $E_c(t)$ and then find the output field $E_{\rm out}(t)$.

B. Results

For the rest of this section, we assume, as in the rest of the paper, that $\alpha=0.95$, $\beta=\pi/2$, and $P_{\rm in}=|\hat{E}_{\rm in}|^2=1$. Additionally, to provide a fair comparison to the single-resonator comb generator, we assume $\gamma_1=\gamma_2=\gamma_3=0$ and $k_1=k_2=k_3=0.03$. Finally, we choose $\widetilde{T}=T/50$ to prioritize the 100 comb lines near the center optical frequency.

Fig. 10 compares the output comb spectrum of a single-ring RE-EO comb generator to the output and reflected comb spectra

of a dual-ring RE-EO comb generator. As expected, the small ring serves as a frequency-dependent coupler, with high transmission at multiples of the small ring FSR, but low transmission at other frequencies. This effect is demonstrated by the reflected spectrum in Fig. 10, where power is concentrated in frequencies at multiples of the small ring FSR.

Fig. 10 also demonstrates why a second output waveguide is crucial to this design. If there is only a single waveguide, the generated comb must then propagate through the smaller coupling ring before being output, causing significant filtering, as shown by the reflected spectrum in Fig. 10. For this reason, in the analysis of Section V-C, we compare the optimal single-ring design, which uses a single waveguide, to the optimal dual-ring design, which uses two waveguides.

The output spectrum from the dual-ring RE-EO comb generator is much higher for comb lines that are within the small ring FSR. The conversion efficiency of input power to the 100 nearest comb lines excluding the center line ($-50 < p < 50$, $p \neq 0$) for the single-ring comb generator is 1.3%, while the conversion efficiency of the dual-ring comb generator is 32.1%. The average increase in output power of these comb lines is 13.9 dB. However, a dip in comb line power occurs at multiples of the small ring FSR because light at these frequencies is coupled efficiently back into the small ring.

The dual-ring comb generator, similar to its single-ring counterpart, requires that the input optical field be resonant with both the smaller coupling ring and the larger comb-generating ring. While the tolerance to optical detuning of the comb-generating ring is high, as shown in Fig. 5(a), the input optical frequency must be more tightly controlled to resonate in the small ring in order to generate high intra-ring optical power. The input optical field will need to be locked within the linewidth of the resonator, which could be achieved by tuning the input optical frequency or by tuning the FSR of the small ring.

Moreover, one possible limitation to the dual-ring comb generator design is the material damage threshold of the small ring. For the parameters discussed above, the time-averaged power in the small ring is 27 times the input optical power. However, even if the input optical power is unrealistically high, such as 1 W, the intra-resonator power is a factor of two below the damage threshold of many state-of-the-art integrated resonators [45].

In some cases, fabricating a ring with a FSR that is 50 times higher than that of the desired comb line spacing may prove challenging due to fabrication constraints. In these cases, it is still possible to generate high-power combs by increasing the size of the ring coupler, but tuning its length so that its FSR is not a harmonic of the FSR of the comb-generating resonator [46]. The resulting FSR of the system is the least common multiple of the two FSRs.

Fig. 11 shows the output spectrum of a dual-ring EO comb generator for various sizes of the small ring and comb-generating resonators, quantified by the ratio of their respective FSRs, $T/\widetilde{T}$. When compared to a small ring coupler ($T/\widetilde{T} = 50$), a larger ring coupler with FSR at a harmonic of the comb-generating resonator ($T/\widetilde{T} = 10$) results in a narrower comb. However, if the FSR of the small ring is adjusted away

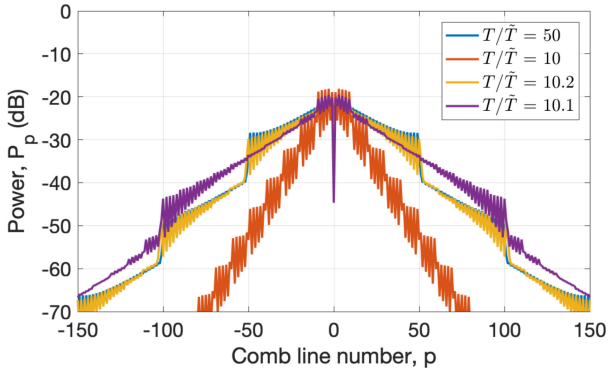

Fig. 11. Output spectra P_p for different values of the ratio of FSRs, $T/\widetilde{T}$, of the small ring and comb-generating resonator. Slightly tuning the FSR of the coupling ring away from a harmonic of the FSR of the comb-generating resonator can increase the comb width and power.

from a harmonic of the comb-generating resonator, the total FSR of the system increases, resulting in broad, high power comb generation without the difficulty of fabricating ultra-small rings. However, this process cannot proceed indefinitely due to the finite linewidth of the small ring resonator. Once the finesse of the ring approaches the ratio of the FSRs, at least one comb line inside the comb-generating resonator will lie inside the linewidth of the small ring. In this case, that comb line will be coupled back into the small ring and the FSR of the entire system will be limited by the small ring FSR.

Finally, we note that it is possible to increase the dual-ring comb conversion efficiency even further by careful optimization of the coupling coefficients. Increasing k_3 will increase the comb conversion efficiency η but also increase the round-trip power loss in the comb-generating ring, r', resulting in an overall increase in the comb slope. In general, the optimal coupling coefficients and coupling ring FSR will depend on the desired number of comb lines and the minimum tolerable power per comb line. However, since the output optical power of a RE-EO comb generator is linearly related to the input optical source power, comb power can be increased simply by using a higher-power source.

C. Application to Optical Communications

As mentioned in Section I, frequency combs can be used in WDM coherent optical communications systems for both the transmitted optical carrier and receiver local oscillator. One problem with single-ring RE-EO comb generators is the low output power in each of the comb lines, which limits the OSNR of the transmitted optical carriers. In this subsection, we briefly analyze the OSNR of WDM optical links utilizing RE-EO comb generators.

Fig. 12 shows an example WDM link that utilizes a RE-EO comb generator that seeds each of the modulated comb frequencies. An input laser is coupled into a RE-EO comb generator where multiple comb lines are generated. The comb is then output-coupled and flattened by an optical filter to reduce power

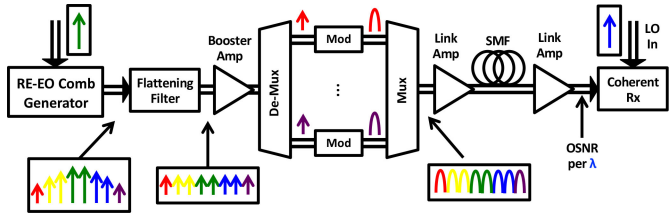

Fig. 12. WDM point-to-point inter-data center link. The output field from the RE-EO comb generator is flattened, amplified, and de-multiplexed (De-mux). Each of the comb lines is modulated (Mod), multiplexed (Mux), and amplified before being input to a link of single-mode fiber (SMF). At the receiving end, the signal is amplified and sent to a coherent receiver (Rx). The OSNR is measured at the receiver input.

TABLE I
WDM LINK PARAMETERS

Input laser power	20 dBm
Insertion loss from output-coupling and flattening	5 dB
Booster amplifier noise figure	5 dB
Booster amplifier gain*	30 dB
Insertion loss from (de-)multiplexing and modulation	20 dB
Link amplifier noise figure	5 dB
Link amplifier gain	20 dB
Insertion loss from SMF	20 dB
Local oscillator power	15 dBm

*20 dB for dual-ring RE-EO comb generator.

fluctuations between comb lines. We note that in this link, the performance is limited by the comb line with the lowest power due to the flat power allocation. The power per comb line after the flattening filter is -20 dBm for the dual-ring link and -30 dBm for the single-ring link. The comb is then amplified with a booster amplifier, and sent to a (de-)multiplexing stage, where the comb lines are separated, modulated individually, and re-combined. After this stage, the comb lines are amplified, transmitted through a length of single-mode fiber (SMF), and amplified before being sent to a coherent receiver.

Table I lists the parameters for this calculation. Here, we assume the link consists of 100 modulated comb lines spaced at 50 GHz, such as in a dense WDM link. However, these results can be easily scaled for links that utilize fewer comb lines or lower-performance devices. For example, for a system that uses amplifiers with a much higher noise figure of 9 dB, the resulting OSNR, reported below, would be reduced by 4 dB. Moreover, it is important to note that a high-power local oscillator is required to achieve the performance stated below. Some link architectures that utilize comb generators at the transmitter and receiver may experience reduced performance due to amplifier noise in the local oscillator.

The difference in booster amplifier power between systems that utilize a single-ring and dual-ring RE-EO comb generator is 10 dB. This performance improvement is smaller than the average comb line power improvement of 14 dB because non-uniformities in the dual-ring RE-EO comb generator output spectrum result in a lower minimum optical power than the single-ring RE-EO comb generator. This effect is evident from the output spectra in Figures 10 and 11.

For the values listed above, we find that the receiver-side OSNR for a single-ring RE-EO comb generator is 21 dB, while the receiver-side OSNR for the dual-ring design is 28 dB. For a typical 28 Gbaud dual-polarization link based on 16-ary quadrature amplitude modulation, the required receiver-side OSNR is $\sim$22 dB [47]. For a WDM link that employs 100 comb lines, as shown in Fig. 10, the total bit-rate per fiber for this system, including overhead is 20 Tb/s. While single-ring RE-EO comb generators can support lower modulation formats, and thus lower bit-rates per fiber, dual-ring comb generators provide an increase in OSNR budget of over 7 dB.

VI. CONCLUSION

Recently, progress in low-loss fabrication techniques and the desire for low-power comb sources has regenerated interest in RE-EO generators. We have developed analytical and numerical methods of predicting the output comb spectrum in the presence of a variety of impairments including optical frequency offsets, modulation frequency offsets, and dispersion. We validate these models against each other and demonstrate that numerical modeling can efficiently approximate the comb spectrum without sacrificing accuracy. However, RE-EO comb generators based on a single resonator often cannot generate enough comb power to be useful for applications such as optical communications. Thus we have proposed a fabricable RE-EO comb generator design that utilizes a ring coupler to enhance the efficiency of the comb generation process. For this new design, the conversion efficiency is 30% higher than designs based on a single resonator, which enable its use in high-capacity coherent optical communications systems.

APPENDIX A
OUTPUT PHASE NOISE

This appendix calculates the relation between the phase noise of the pth comb line and the phase noise of the input optical field for resonant operation, as discussed in Section II-B. We first assume that the input optical field is $E_{\rm in}(t) = \hat{E}_{\rm in} e^{i\omega_0 t + i\theta_o(t)}$, with PSD, $S_{\rm in}(\omega)$, given by (7). The PSD of the output field, $E_{\rm out}(t)$ is

$$\begin{aligned} S_{out}(\omega) &= \int_{-\infty}^{\infty} \langle E_{\rm out}(t) E^*_{\rm out}(t+\tau)\rangle e^{-i\omega\tau} d\tau \\ &= (1-\gamma)(1-k) S_{\rm in}(\omega) - (1-\gamma) k S_{o,1}(\omega) \\ &\quad - (1-\gamma) k S_{o,2}(\omega) + (1-\gamma)\frac{k^2}{1-k} S_{o,3}(\omega), \end{aligned} \tag{33}$$

where $S_{o,1}(\omega)$, $S_{o,2}(\omega)$, and $S_{o,3}(\omega)$ result from the autocorrelation of $E_{\rm out}(t)$, given by (5), and are

$$\begin{aligned} S_{o,1}(\omega) = \int_{-\infty}^{\infty} \Bigg\langle E_{\rm in}(t) \sum_{n=1}^{\infty} r^n e^{-i\beta n \sin\omega_m(t+\tau)} \\ \times E^*_{\rm in}(t+\tau-nT) \Bigg\rangle e^{-i\omega\tau} d\tau \end{aligned} \tag{34}$$

$$S_{o,2}(\omega) = \int_{-\infty}^{\infty} \left\langle E_{\text{in}}^*(t+\tau) \sum_{n=1}^{\infty} r^n e^{i\beta n \sin\omega_m t} \times E_{\text{in}}(t-nT) \right\rangle e^{-i\omega\tau} d\tau \quad (35)$$

$$S_{o,3}(\omega) = \int_{-\infty}^{\infty} \left\langle \sum_{n,m=1}^{\infty} r^{n+m} e^{i\beta n \sin\omega_m t} e^{-i\beta m \sin\omega_m (t+\tau)} \times E_{\text{in}}(t-nT) E_{\text{in}}^*(t+\tau-mT) \right\rangle e^{-i\omega\tau} d\tau. \quad (36)$$

Focusing first on $S_{o,1}(\omega)$ and $S_{o,2}(\omega)$, we note that the optical phase noise is uncorrelated to the phase modulation and thus the time-averaging inside the integrals can be separated into two terms, i.e.,

$$\left\langle E_{\text{in}}(t) \sum_{n=1}^{\infty} r^n e^{-i\beta n \sin\omega_m (t+\tau)} E_{\text{in}}^*(t+\tau-nT) \right\rangle = \sum_{n=1}^{\infty} r^n \langle e^{-i\beta n \sin\omega_m (t+\tau)} \rangle \langle E_{\text{in}}(t) E_{\text{in}}^*(t+\tau-nT) \rangle. \quad (37)$$

A Jacobi-Anger expansion can be applied to terms similar to the leftmost expectation above, resulting in

$$\langle e^{\pm i\beta n \sin\omega_m (t+\tau)} \rangle = \left\langle \sum_{p=-\infty}^{\infty} J_p(\beta n) e^{\pm ip\omega_m (t+\tau)} \right\rangle = J_0(\beta n). \quad (38)$$

With some algebra, the following expressions can be obtained for $S_{o,1}(\omega)$ and $S_{o,2}(\omega)$ as a function of the input PSD $S_{\text{in}}(\omega)$:

$$S_{o,1}(\omega) = \left[\sum_{n=1}^{\infty} r^n J_0(\beta n) e^{-i\omega nT} \right] S_{\text{in}}(\omega) \quad (39)$$

$$S_{o,2}(\omega) = \left[\sum_{n=1}^{\infty} r^n J_0(\beta n) e^{i\omega nT} \right] S_{\text{in}}(\omega) \quad (40)$$

To calculate $S_{o,3}(\omega)$, we separate uncorrelated terms, similar to (37), resulting in the following simplification:

$$\langle e^{i\beta n \sin\omega_m t} e^{-i\beta m \sin\omega_m (t+\tau)} \rangle = \left\langle \sum_{p,q=-\infty}^{\infty} J_p(\beta n) J_q(\beta m) e^{i(p-q)\omega_m t} e^{-iq\omega_m \tau} \right\rangle = \sum_{p=-\infty}^{\infty} J_p(\beta n) J_p(\beta m) e^{-ip\omega_m \tau}. \quad (41)$$

With some additional algebra, we can express $S_{o,3}(\omega)$ as a function of $S_{\text{in}}(\omega)$,

$$S_{o,3}(\omega) = \sum_{p=-\infty}^{\infty} S_{\text{in}}(\omega - p\omega_m) \times \left[\sum_{n,m=1}^{\infty} r^{n+m} J_p(\beta n) J_p(\beta m) e^{i\omega(n-m)T} \right]. \quad (42)$$

Finally, the output PSD is

$$S_{out}(\omega) = (1-\gamma)\big[(1-k) - 2\,kRe\{\chi_0(\omega)\}\big] S_{\text{in}}(\omega) + (1-\gamma)\frac{k^2}{1-k} \sum_{p=-\infty}^{\infty} \big|\chi_p(\omega)\big|^2 S_{\text{in}}(\omega - p\omega_m), \quad (43)$$

where we have defined the linewidth correction term $\chi_p(\omega)$ in (9).

Appendix B
Modulation Frequency Offset

This section derives the power in the pth comb line in the presence of modulation frequency offsets, as defined in Section III-B. First, in the presence of modulation frequency offsets, we can adjust the cascaded modulation function, (2), to include the modulation frequency offset $\phi_m = \Delta\omega_m T$ by noting

$$\begin{aligned} \beta F_n(\omega_m t) &= \beta \sum_{i=1}^{n} \sin\omega_m (t - iT) \\ &= \beta \sin(\omega_m t)\left(\frac{1}{2}\cot(\phi_m/2) - \frac{\cos((n+\frac{1}{2})\phi_m)}{2\sin(\phi_m/2)} \right) \\ &\quad - \beta\cos(\omega_m t)\left(-\frac{1}{2} + \frac{\sin((n+\frac{1}{2})\phi_m)}{2\sin(\phi_m/2)} \right) \\ &= \beta_o(\phi_m, n)\sin(\omega_m t) - \beta_e(\phi_m, n)\cos(\omega_m t), \end{aligned} \quad (44)$$

where in the second line we used Lagrange's trigonometric identities and have simplified the final expression using $\beta_o(\phi_m, n)$ and $\beta_e(\phi_m, n)$ as defined in Section III-B.

We can then insert this expression into (1) and find an expression for the output optical field in a similar manner to that of (5):

$$\begin{aligned} E_{\text{out}}(t) &= \sqrt{(1-\gamma)(1-k)}\hat{E}_{\text{in}} e^{i\omega_0 t} - k\sqrt{\frac{1-\gamma}{1-k}}\hat{E}_{\text{in}} e^{i\omega_0 t} \\ &\quad \times \sum_{n=1}^{\infty} \left(r^n e^{-i\beta_o(\phi_m,n)\sin(\omega_m t)} e^{-i\beta_o(\phi_m,n)\cos(\omega_m t)} \right) \\ &= \sqrt{(1-\gamma)(1-k)}\hat{E}_{\text{in}} e^{i\omega_0 t} \left[1 - \frac{k}{1-k} \sum_{p=-\infty}^{\infty} e^{ip\omega_m t} \right. \\ &\quad \left. \times \sum_{n=1}^{\infty} \sum_{q=-\infty}^{\infty} r^n i^q J_{p-q}(\beta_o(\phi_m, n)) J_q(\beta_e(\phi_m, n)) \right]. \end{aligned} \quad (45)$$

From this output field, composed of equidistant frequencies spaced at the modulation frequency, we can calculate the output power in the pth comb line, given by (15). When the modulator frequency is tuned exactly to the resonator FSR ($\phi_m = 0$), this result reduces to (6).

Acknowledgment

The authors are grateful for helpful discussions with Prof. S. E. Harris.

REFERENCES

[1] H. Ye, H. Schnatz, and L. W. Hollberg, "Optical frequency combs: From frequency metrology to optical phase control," *IEEE J. Sel. Topics Quantum Electron.*, vol. 9, no. 4, pp. 1041–1058, Jul. 2003.

[2] I. Coddington, N. Newbury, and W. Swann, "Dual-comb spectroscopy," *Optica*, vol. 3, no. 4, pp. 414–426, Apr. 2016.

[3] P. J. Delfyett *et al.*, "Optical frequency combs from semiconductor lasers and applications in ultrawideband signal processing and communications," *J. Lightw. Technol.*, vol. 24, no. 7, Jul. 2006, Art. no. 2701.

[4] H. Telle, G. Steinmeyer, A. Dunlop, J. Stenger, D. Sutter, and U. Keller, "Carrier-envelope offset phase control: A novel concept for absolute optical frequency measurement and ultrashort pulse generation," *Appl. Phys. B*, vol. 69, no. 4, pp. 327–332, Oct. 1999.

[5] G. Millot *et al.*, "Frequency-agile dual-comb spectroscopy," *Nature Photon.*, vol. 10, no. 1, pp. 27–30, 2016.

[6] H. A. Haus, "Mode-locking of lasers," *IEEE J. Sel. Topics Quantum Electron.*, vol. 6, no. 6, pp. 1173–1185, 2000.

[7] E. Myslivets, B. P. Kuo, N. Alic, and S. Radic, "Generation of wideband frequency combs by continuous-wave seeding of multistage mixers with synthesized dispersion," *Opt. Express*, vol. 20, no. 3, pp. 3331–3344, Jan. 2012.

[8] P. Del'Haye, A. Schliesser, O. Arcizet, T. Wilken, R. Holzwarth, and T. J. Kippenberg, "Optical frequency comb generation from a monolithic microresonator," *Nature*, vol. 450, Dec. 2007.

[9] T. J. Kippenberg, R. Holzwarth, and S. A. Diddams, "Microresonator-based optical frequency combs," vol. 332, no. 6029, pp. 555–559, 2011.

[10] J. Pfeifle *et al.*, "Coherent terabit communications with microresonator kerr frequency combs," *Nature Photon.*, vol. 8, no. 5, pp. 375–380, 2014.

[11] P. Marin-Palomo *et al.*, "Microresonator-based solitons for massively parallel coherent optical communications," *Nature*, vol. 546, pp. 274–279, Jun. 2017.

[12] T. Herr *et al.*, "Universal formation dynamics and noise of kerr-frequency combs in microresonators," *Nature Photon.*, vol. 6, pp. 480–487, Jun. 2012.

[13] A. Fülöp *et al.*, "Frequency noise of a normal dispersion microresonator-based frequency comb," in *Proc. Opt. Fiber Commun. Conf.*, Optical Society of America, 2017, Paper W2A.6.

[14] R. Wu, V. R. Supradeepa, C. M. Long, D. E. Leaird, and A. M. Weiner, "Generation of very flat optical frequency combs from continuous-wave lasers using cascaded intensity and phase modulators driven by tailored radio frequency waveforms," *Opt. Lett.*, vol. 35, no. 19, pp. 3234–3236, Oct. 2010.

[15] A. J. Metcalf, V. Torres-Company, D. E. Leaird, and A. M. Weiner, "High-power broadly tunable electrooptic frequency comb generator," *IEEE J. Sel. Topics Quantum Electron.*, vol. 19, no. 6, pp. 231–236, Nov. 2013.

[16] S. T. Cundiff, J. Ye, and J. L. Hall, "Optical frequency synthesis based on mode-locked lasers," *Rev. Scientific Instrum.*, vol. 72, no. 10, pp. 3749–3771, 2001.

[17] T. Kobayashi, T. Sueta, Y. Cho, and Y. Matsuo, "High-repetition-rate optical pulse generator using a fabry-perot electro-optic modulator," *Appl. Phys. Lett.*, vol. 21, no. 8, pp. 341–343, 1972.

[18] K. P. Ho and J. M. Kahn, "Optical frequency comb generator using phase modulation in amplified circulating loop," *IEEE Photon. Technol. Lett.*, vol. 5, no. 6, pp. 721–725, Jun. 1993.

[19] M. Kourogi, K. Nakagawa, and M. Ohtsu, "Wide-span optical frequency comb generator for accurate optical frequency difference measurement," *IEEE J. Quantum Electron.*, vol. 29, no. 10, pp. 2693–2701, Oct. 1993.

[20] T. Saitoh *et al.*, "Modulation characteristic of waveguide-type optical frequency comb generator," *J. Lightw. Technol.*, vol. 16, no. 5, pp. 824–832, May 1998.

[21] S. Bennett, B. Cai, E. Burr, O. Gough, and A. J. Seeds, "1.8-thz bandwidth, zero-frequency error, tunable optical comb generator for dwdm applications," *IEEE Photon. Technol. Lett.*, vol. 11, no. 5, pp. 551–553, May 1999.

[22] Y. Ma, Q. Yang, Y. Tang, S. Chen, and W. Shieh, "1-tb/s single-channel coherent optical ofdm transmission with orthogonal-band multiplexing and subwavelength bandwidth access," *J. Lightw. Technol.*, vol. 28, no. 4, pp. 308–315, Feb. 2010.

[23] M. Zhang, C. Wang, R. Cheng, A. Shams-Ansari, and M. Lončar, "Monolithic ultra-high-q lithium niobate microring resonator," *Optica*, vol. 4, no. 12, pp. 1536–1537, Dec. 2017.

[24] M. Zhang *et al.*, "Broadband electro-optic frequency comb generation in a lithium niobate microring resonator," *Nature*, vol. 568, no. 7752, pp. 373–377, 2019.

[25] A. Rueda, F. Sedlmeir, M. Kumari, G. Leuchs, and H. G. L. Schwefel, "Resonant electro-optic frequency comb," *Nature*, vol. 568, no. 7752, pp. 378–381, 2019.

[26] M. Kourogi, B. Widiyatomoko, Y. Takeuchi, and M. Ohtsu, "Limit of optical-frequency comb generation due to material dispersion," *IEEE J. Quantum Electron.*, vol. 31, no. 12, pp. 2120–2126, Dec. 1995.

[27] A. S. Bell, G. M. Mcfarlane, E. Riis, and A. I. Ferguson, "Efficient optical frequency-comb generator," *Opt. Lett.*, vol. 20, no. 12, pp. 1435–1437, Jun. 1995.

[28] M. Kourogi, T. Enami, and M. Ohtsu, "A coupled-cavity monolithic optical frequency comb generator," *IEEE Photon. Technol. Lett.*, vol. 8, no. 12, pp. 1698–1700, Dec. 1996.

[29] M. Zhang, C. Wang, B. Buscaino, A. Shams-Ansari, J. M. Kahn, and M. Loncar, "Electro-optic frequency comb generation in ultrahigh-Q integrated lithium niobate micro-resonators," in *Proc. Conf. Lasers Electro-Opt., QELS Fundamental Sci.*, Optical Society of America, 2018, Paper FW3E.4.

[30] S. Xiao, L. Hollberg, N. R. Newbury, and S. A. Diddams, "Toward a low-jitter 10 ghz pulsed source with an optical frequency comb generator," *Opt. Express*, vol. 16, no. 12, pp. 8498–8508, Jun. 2008.

[31] M. Abramowitz, I. A. Stegun, and M. David, *Handbook of Mathematical Functions with Formulas, Graphs, and Mathematical Tables* (National Bureau of Standards Applied Mathematics Series No. 55). 1965.

[32] J. G. Proakis and M. Salehi, *Digital Communications*. New York: McGraw-Hill, vol. 4, 2001.

[33] G. P. Agrawal, *Fiber-Optic Communication Systems*, vol. 222. Hoboken, NJ, USA: Wiley, 2012.

[34] K.-P. Ho, "Optical frequency comb generator using phase modulation in amplified circulating loop," M. S. Thesis, University of California, Berkeley, Berkeley, CA, 1993.

[35] J. Craninckx and M. Steyaert, "Low-noise voltage-controlled oscillators using enhanced lc-tanks," *IEEE Trans. Circuits Syst. II: Analog Digit. Signal Process.*, vol. 42, no. 12, pp. 794–804, Dec. 1995.

[36] J. Kim, D. J. Richardson, and R. Slavík, "Cavity-induced phase noise suppression in a fabry–perot modulator-based optical frequency comb," *Opt. Lett.*, vol. 42, no. 8, pp. 1536–1539, Apr. 2017.

[37] S. Xiao, L. Hollberg, and S. A. Diddams, "Generation of a 20 ghz train of subpicosecond pulses with a stabilized optical-frequency-comb generator," *Opt. Lett.*, vol. 34, no. 1, pp. 85–87, Jan. 2009.

[38] S. Harris and O. McDuff, "Theory of FM laser oscillation," *IEEE J. Quantum Electron.*, vol. 1, no. 6, pp. 245–262, Sep. 1965.

[39] S. E. Harris and B. J. McMurtry, "Frequency selective coupling to the FM laser," *Appl. Phys. Lett.*, vol. 7, no. 10, pp. 265–267, 1965.

[40] A. E. Siegman and D. J. Kuizenga, "Active mode-coupling phenomena in pulsed and continuous lasers," *Opto-electronics*, vol. 6, no. 1, pp. 43–66, Jan. 1974.

[41] J. Heebner, R. Grover, T. Ibrahim, and T. A. Ibrahim, *Optical Microresonators: Theory, Fabrication, and Applications*, vol. 138. New York; Berlin: Springer Science & Business Media, 2008.

[42] R. P. Kovacich, U. Sterr, and H. R. Telle, "Short-pulse properties of optical frequency comb generators," *Appl. Opt.*, vol. 39, no. 24, pp. 4372–4376, Aug. 2000.

[43] Z. Jiang *et al.*, "Spectral line-by-line pulse shaping on an optical frequency comb generator," *IEEE J. Quantum Electron.*, vol. 43, no. 12, pp. 1163–1174, Dec. 2007.

[44] Y. He, H. Liang, R. Luo, M. Li, and Q. Lin, "Dispersion engineered high quality lithium niobate microring resonators," *Opt. Express*, vol. 26, no. 13, pp. 16 315–16 322, Jun. 2018.

[45] C. Wang, M. Zhang, M. Yu, R. Zhu, H. Hu, and M. Loncar, "Monolithic lithium niobate photonic circuits for kerr frequency comb generation and modulation," *Nature Commun.*, vol. 10, no. 1, Art. no. 978, 2019.

[46] S. A. Miller *et al.*, "Tunable frequency combs based on dual microring resonators," *Opt. Express*, vol. 23, no. 16, pp. 21 527–21 540, Aug. 2015.

[47] J. K. Perin, A. Shastri, and J. M. Kahn, "Data center links beyond 100 gbit/s per wavelength," *Opt. Fiber Technol.*, vol. 44, pp. 69–85, 2018, special Issue on Data Center Communications.

Brandon Buscaino (Student Member, IEEE) received the B.S. degree in physics, in 2015, and the M.S. degree in electrical engineering, in 2016, both from Stanford University, Stanford, CA, USA, where he is currently working toward the Ph.D. degree with Stanford University. His current research interests include coherent optical fiber communications, intra-data center link design, and co-packaged optical interfaces.

Mian Zhang (Member, IEEE) received the B.S. degree in physics from the University of Bristol, Bristol, U.K, in 2009, and the Ph.D. degree in applied and engineering physics from Cornell University, Ithaca, NY, USA, in 2015. Between 2015 and 2018, he was a Postdoctoral Fellow with Harvard University where he demonstrated an ultrahigh performance integrated photonics platform using thin-film lithium niobate. His research interests include integrated photonics, electro-optics, and nonlinear optics. He founded HyperLight Corporation, commercializing integrated lithium niobate photonic circuits technology, in 2018 where he currently serves as CEO.

Marko Lončar (Senior Member, IEEE) is the Tiantsai Lin Professor of Electrical Engineering with Harvard John A. Paulson School of Engineering and Applied Sciences (SEAS), as well as a Harvard College Professor. He received the diploma from the University of Belgrade, Belgrade, Serbia, in 1997 and the Ph.D. degree from Caltech, Pasadena, CA, USA, in 2003, both in electrical engineering. After completing his Postdoctoral studies at Harvard, he joined SEAS Faculty in 2006. He is an expert in nanophotonics and nanofabrication. His current research interests include quantum and nonlinear nanophotonics, quantum optomechanics, and nanofabrication. He is the recipient of Sloan Fellowship (2010) and Levenson Prize for Excellence in Undergraduate Teaching (2012). He is a Fellow of Optical Society of America, and a senior member of SPIE.

Joseph M. Kahn (Fellow, IEEE) received the A.B., M.A., and Ph.D. degrees in physics from the University of California, Berkeley, CA, USA in 1981, 1983, and 1986. In 1987–1990, he was with AT&T Bell Laboratories. In 1989, he demonstrated the first successful synchronous (i.e., coherent) detection in optical fiber systems, achieving record receiver sensitivity. In 1990–2003, he was on the Electrical Engineering and Computer Sciences Faculty at Berkeley. He demonstrated coherent detection of QPSK in 1992. In 1999, D.-S. Shiu and he authored the first work on shaping and nonequiprobable signaling for optical communications. In the 1990 s and early 2000 s, he and his collaborators performed seminal work on indoor and outdoor free-space optical communications and multi-input–multi-output wireless communications. In 2000, he and K.-P. Ho founded StrataLight Communications, whose 40 Gb/s-per-wavelength long-haul fiber transmission systems were deployed widely by AT&T, Deutsche Telekom, and other carriers. In 2002, Ho and he applied to patent the first electronic compensation of fiber Kerr nonlinearity. StrataLight was acquired by Opnext in 2009. In 2003, he became a Professor of electrical engineering in the E. L. Ginzton Laboratory with Stanford University. He and his collaborators have extensively studied rate-adaptive coding and modulation, as well as digital signal processing for mitigating linear and nonlinear impairments in coherent systems. In 2008, E. Ip and he (and G. Li independently) invented simplified digital backpropagation for compensating fiber Kerr nonlinearity and dispersion. Since 2004, he and his collaborators have been studied propagation, modal statistics, spatial multiplexing and imaging in multi-mode fibers, elucidating principal modes and demonstrating transmission beyond the traditional bandwidth-distance limit in 2005, deriving the statistics of coupled modal group delays and gains in 2011, and deriving resolution limits for imaging in 2013. His current research interests include optical frequency comb generators, coherent data center links, rate-adaptive access networks, fiber Kerr nonlinearity mitigation, ultra-long-haul submarine links, and optimal free-space transmission through atmospheric turbulence. He was the recipient of the National Science Foundation Presidential Young Investigator Award in 1991.